Silver nanoparticles embedded hybrid organometallic complexes: Structural interactions, photo-induced energy transfer, plasmonic effect and optical thermometry

Cite as: AIP Advances **8**, 065117 (2018); https://doi.org/10.1063/1.5020812
Submitted: 27 December 2017 . Accepted: 04 June 2018 . Published Online: 27 June 2018

Praveen Kumar Shahi, Rajiv Prakash, and Shyam Bahadur Rai

Silver nanoparticles embedded hybrid organometallic complexes: Structural interactions, photo-induced energy transfer, plasmonic effect and optical thermometry

Praveen Kumar Shahi,[1,2,a] Rajiv Prakash,[3] and Shyam Bahadur Rai[1]
[1]*Department of Physics, Banaras Hindu University, Varanasi 221005, India*
[2]*Department of Physics, SPM Government Degree College, Allahabad 211013, India*
[3]*School of Material Science and Engineering, IIT (BHU), Varanasi 221005, India*

(Received 27 December 2017; accepted 4 June 2018; published online 27 June 2018)

A novel hybrid material comprising of two β-diketonate complexes, $Tb(ASA)_3Phen$ (TAP) and $Eu(TTA)_3Phen$ (ETP), has been synthesized and studied its photo-physics, energy transfer and optical thermometry applications. Using XRD and FTIR spectra, it has been demonstrated that both the complexes maintain their core entity and show weak interaction between them in the hybrid complex (HC). The TEM images show the coating of ETP layers over nano-fibrous TAP and further, embedded with Ag nanoparticles over HC. It has been observed that ligands (Phen, TTA as well as ASA) absorb the UV radiation and undergoes single to triplet via intersystem crossing transitions by transferring its excitation energy to central lanthanide ions (Eu^{3+} and Tb^{3+}). In this strategy, an efficient energy transfer between two different species i.e. ASA to Tb^{3+} (in TAP complex) to Eu^{+3} ions (of ETP complex) has also been observed. To probe and verify the energy transfer mechanism, life time measurements have been carried out. The life time of Tb^{3+} decreases in HC as compared with TAP, whereas the life time of Eu^{3+} increases in HC as compared with ETP. The addition of silver nanoparticles (AgNPs) again enhances the fluorescence intensity of Eu^{3+} emission band. The prepared HC has further been demonstrated for ambient range temperature (295-365 K) sensing and the sensitivity of the material is found to be 6.8% change in signal per K. The strong optical property and non-toxic nature of this HC is useful in biomedical, bio-imaging and energy harvesting applications. https://doi.org/10.1063/1.5020812

I. INTRODUCTION

Lanthanide compounds specially organic-inorganic hybrid fluorophores have become a very wide, active and attractive field of intense research due to their multifunctional and versatile properties as well as wide range of practical applications in day-to-day life.[1–5] Their excellent optical properties such as large Stokes' shifted emission, high quantum yield, narrow bandwidth, long lived decay profile and mechanical flexibility offer promising applications in many fields such as sensors, in medical diagnostics, optical and electronic devices etc.[1–10] Lanthanide complexes are basically organo-metallic complexes, in which organic ligands and the rare-earth ion are bonded either through covalent or co-ordinate bonds. The recent trends in the field of lanthanide complexes are to introduce metal nanoparticles to tune its luminescent behavior and boost their efficiency for optical device applications.[11–14] Recently, Parola et al. have given a detailed overview on different types of lanthanide based hybrid nanomaterials and demonstrated that, controlled coupling between plasmonics (attaching metal nanoparticles) and luminescence opens a wide field of intense research.[15]

[a]**Corresponding authors-Praveen Kumar Shahi** (praveenkshahi@gmail.com)

The luminescence mechanism of the lanthanide complexes are based on the ligand absorption coefficient and energy transfer to central metal ion (lanthanides). The absorption coefficients of organic ligands in UV-blue region are very high, further the energy transfer from the ligands to the central metal ions (known as antenna effect) takes place.[16,17] The spherical cavity of organic ligands facilitates encapsulation of central metal ions.[16,17] Therefore, the optical properties of lanthanide complexes can be modulated by introducing one or more type of ligands as well as selection of one or more type of rare earth ions.[18–21] In case of $Tb_xEu_{1-x}(aspirin)_3Phen$, Zhang et al. have reported that the PL intensity of Eu^{3+} ion increases with increasing the Tb^{3+} concentration through energy transfer process.[22] In case of $Tb_{1-x}Eu_x(TTA)_3Phen$ complex, Lu et al. have also shown an enhancement in emission intensity of Eu^{3+} ion in the presence of Tb^{3+} ion.[23] However, to the best of our knowledge, there is no report showing interaction and the energy transfer mechanism between the two different metal-organic complexes. The strategy to enhance the fluorescence efficiency of Eu^{3+} ions can be extended by introducing more than one absorbing ligands. The objective of present work was to introduce different organic ligands (energy harvesters) along with Tb^{3+} ion to get maximum PL intensity of Eu^{3+} ion through cascade energy transfer.

Among the various organic ligands, β-diketonates possess large UV absorption coefficient, good coordination with central metal ions and large energy transfer efficiency.[24–27] In our previous report we have demonstrated the multi-functionality of red emitting $Eu(TTA)_3Phen$ (ETP) complexes, in which TTA molecules absorbed the UV-A as well as UV-B part of the radiation and transfer its energy to central Eu^{3+} ion, whereas Phen protect it from the interaction with water molecules and thus provides stability to the complex.[6,28] Recently, Kumar et al. have reported a strong green emitting $Tb(ASA)_3Phen$ (TAP) complex, in which acetylsalicylic acid (ASA) serves as the UV harvesting ligands.[27] In the present work, a hybrid complex (HC) by the mixing of ETP and TAP complexes has been prepared and their structural and optical properties have been investigated in details. Such a hybrid system combines the properties of both the complexes and offers an efficient energy transfer from Tb^{3+} to Eu^{3+} ions. Along with this, an energy transfer from ASA to Eu^{3+} ion has also been observed.

In order to further enhance the PL intensity of Eu^{3+} ion, surface Plasmon-enhanced fluorescence strategy has been adopted. In the presence of metallic nanoparticles (Ag, Au, Cu, Bi), the emission enhancement due to the plasmonic effect may occur because of the increase in absorption rate by the local field enhancement effect. That results increment in fluorescence intensity directly associated with enhanced decay rates.[29–31] Wang et al. fabricated truncated triangular silver nanoprisms and made a theoretical as well as experimental investigation about the influence of these nanoprisms on the fluorescence property of europium complex $Eu(TTFA)_3$.[32] They found that the emission intensity of Eu^{3+} in the complex is greatly enhanced through minimization of the nonradiative decay losses. Li et al. successfully synthesized the Au nanoparticle@mSiO2@PABI-Eu nanocomposite and their spectroscopic results revealed that the emission intensity of the Au nanoparticle@mSiO2@PABI-Eu nanocomposite is highly dependent on the thickness of silica layer.[33] Sudheendra et al. prepared a photonic material with plasmonic and up-converting properties by coating gold onto the surface of a fluoride matrix to see the plasmonic effect.[34] Fang et al. observed luminescence enhancement and quenching in $Eu(TTA)_3.H_2O$ complex in the presence of silver nanoparticles depending on the concentration of Ag nanoparticles as well as complex molecule.[35] The Ag nanoparticles increase the electronic-dipole transition rate due to enhanced local field surrounding Eu^{3+} ions, while the nonradiative transition rate decreased owing to decreased resonant energy transfer among europium complex molecules. These two factors lead to the luminescence enhancement of europium complex. However, at the lower concentration of the Eu-complex luminescence quenching takes place due to the absorption competition between Ag nanoparticles and the europium complex. We have used silver nanoparticles to modify the luminescence property of Tb^{3+} and Eu^{3+} ions. The significant difference between the narrow absorption of AgNPs with absorption band of complex; reduces the possibility of absorption competition between the complexes and the AgNPs with the UV excitation wavelengths. A maximum two-fold luminescence enhancement in the presence of AgNPs was observed. Furthermore, this material shows high-temperature sensitivity (295-365K), photostability and excellent brightness.

II. MATERIALS

Europium (III) oxide (99.999%, Alfa Aesar), terbium (III) oxide (99.999%, Alfa Aesar), acetylsalicylic acid (98%, Alfa Aesar), 2-theonyltrifluoroacetone (99.5%, Otto Kemi), 1,10-phenanthroline (99%, Alfa Aesar), silver nitrate (99.99, Alfa Aesar), sodium borohydride (99.5%, Loba Chemie, Pvt. Ltd.), ethanol (Merck), sodium hydroxide (Qualigens, 99), hydrochloric acid (Fisher Scientific) and cyclohexane (Fisher Scientific) were used for the synthesis of complexes and HC. These materials were used without any further processing and purification.

III. METHODOLOGY

A. Material synthesis

1. Synthesis of Eu-complex ($Eu(TTA)_3Phen$)

The $Eu(TTA)_3Phen$ complex has been synthesized using solution caste technique; reported in our previous reports.[6,28]

2. Synthesis of Tb-complex ($Tb(ASA)_3Phen$)

A solution of ASA (6 mmol) and 1,10-phenanthroline (Phen) (2 mmol) in 30 ml of ethanol was prepared. The pH value of the solution was adjusted to 7 by the addition of NaOH. In the next step, another solution of $TbCl_3{\cdot}6H_2O$ (2 mmol) in 10 ml of distilled water was drop wise added into the first one under constant stirring. The obtained white precipitate was collected by centrifugation and washed thrice with ethanol and dried under vacuum at 313 K for 24 h.

3. Synthesis of hybrid complex (HC)

In order to prepare HC, a mixture of $Eu(TTA)_3Phen$ and $Tb(ASA)_3Phen$ in equal molar amount (1:1 mmol) were taken and dispersed in 30 ml of cyclohexane. Further, the mixture was stirred vigorously for about 6 h and kept in ultrasonic bath for about 1 h to get proper dispersion and mixing. Then, the prepared HC has been collected by centrifugation and dried under vacuum at 313 K for 24 h.

4. Synthesis of AgNPs and AgNPs attached HC

AgNPs have been prepared by reduction of silver nitrate by ice-cold sodium borohydride.[36] Sodium borohydride reduces the silver nitrate and stabilize the formed nanoparticles. A 30 ml of 0.001 M sodium borohydride aqueous solution was chilled in an ice bath. The reaction mixture was stirred vigorously on a magnetic stirrer. Then 2 ml of 0.001 M silver nitrate ($AgNO_3$) was added in the ice-child $NaBH_4$ solution slowly (1 drop per second). The solution turned brighter yellow after the complete addition of $AgNO_3$, the stirring stopped immediately. Further, different concentrations (0 ml, 1 ml, 2 ml and 4 ml) of the prepared AgNPs were mixed physically in the 20 mmol dispersed aqueous solution of HC. The mixture was then ultra-sonicated about 30 minutes for the better dispersion of AgNPs with HC. The prepared hybrid nanoparticles (HNPs) was then collected by centrifugation and dried in vacuum oven at 313 K overnight. The complete synthesis process is illustrated in Fig. 1.

B. Instrumentation

Transmission electron microscopy (TEM) images were captured using FEI, Tecnai G2, S-Twin instrument operating at 200 kV. Elemental composition analysis was carried out using an energy dispersive x-ray analysis unit (EDAX, model: Zeiss EVO 18 Research). XRD patterns were measured using an x-ray diffractometer (Model: Miniflex-II, Rigaku, Japan) with CuKα radiation (λ = 1.5406 Å). Fourier transform infrared (FTIR) spectroscopy measurements were carried out using FTIR from Perkin Elmer (model no: Spectrum-65) in the range of 400-4000 cm^{-1}. The UV-Vis-NIR absorption spectra were recorded by using Lambda-750 UV-visible-NIR spectrophotometer from Perkin Elmer. Photoluminescence/excitation (PL/E) and lifetime measurements were performed using spectrometer (model: FL3-11, Horiba Jobin Yvon) equipped with 450 W CW Xe-lamp and 25 W pulsed Xe-lamp. In order to be able to measure the PL in the ambient temperature range a

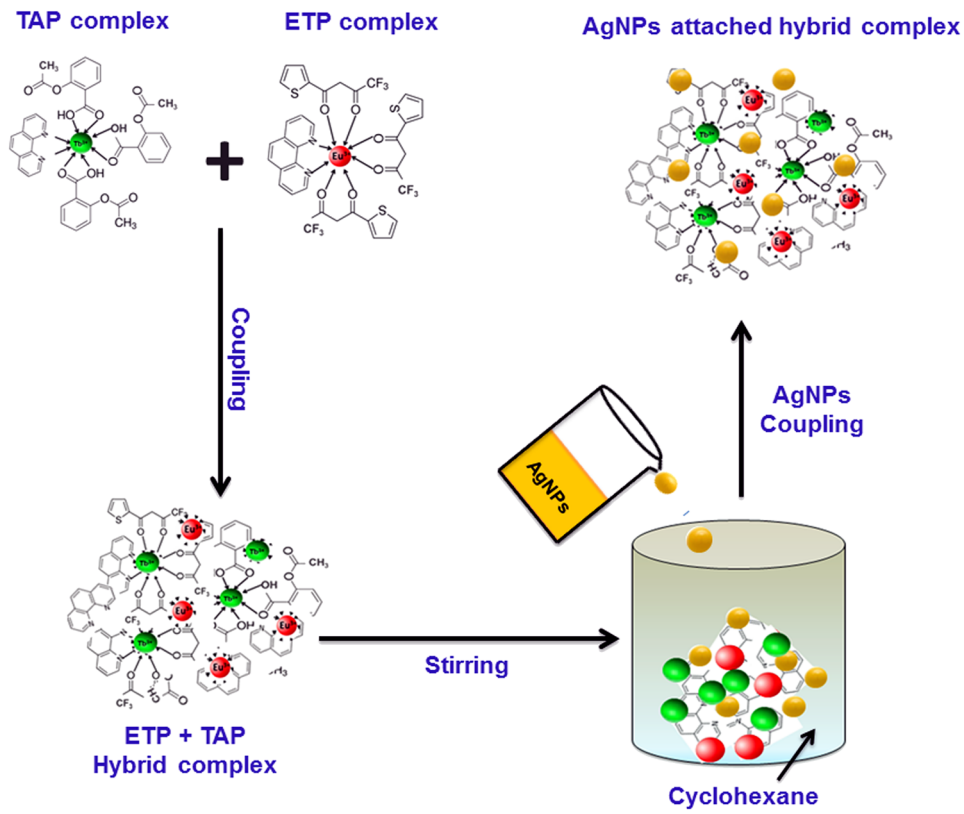

FIG. 1. A schematic illustration for the attachment of AgNPs with HC.

standard heating equipment (Torsion Spinot DIGITAL Stirrer MC02) was used and excited with the MDL-III-405. The PL with temperature was recorded using the Ocean Optics QE 65000 (CCD) attached with optical fiber.

IV. RESULTS AND DISCUSSION

A. Structural characterization using XRD and FTIR

To confirm the possible interaction between the two complexes, we have carried out the x-ray diffraction (XRD) and infrared spectroscopic (FTIR) measurements. Fig. 2 shows the XRD pattern of ETP, TAP and HC. The x-ray diffraction peaks corresponding to both ETP and TAP complexes are present in the HC, indicating the presence of both the phases in hybrid formation.

The crystalline size of TAP complex and HC have been estimated using Debye Scherer's formula-

$$D = 0.9\lambda/\beta cos\theta$$

Where D is the average grain size of the crystallites, λ is the wavelength of Cu-Kα radiation (1.54Å), β is the corrected full width at half maximum (FWHM) of the diffraction peak in radians and θ is the diffraction angle. The crystallite size is found to be about 20 and 22 nm for TAP complex and HC, respectively.

To confirm the possible interaction between the two complexes, we have carried out the infrared spectroscopic measurements. To probe further interaction between ETP and TAP complexes in HC, FTIR measurement has been carried out. Fig. 3 shows the FTIR spectra of ETP, TAP and HC. FTIR spectra of ETP contains large number of absorption peaks which are basically due to three constituent molecules in ETP namely phen, TTA and Eu-O, that has already been discussed in our previous report.[6] The fingerprint IR peak of TTA is observed at 1600 cm^{-1} which is due to asymmetric stretching mode of C=O.[37] Theonyl ring in the TTA structure points at 1413 cm^{-1} and 1540 cm^{-1}

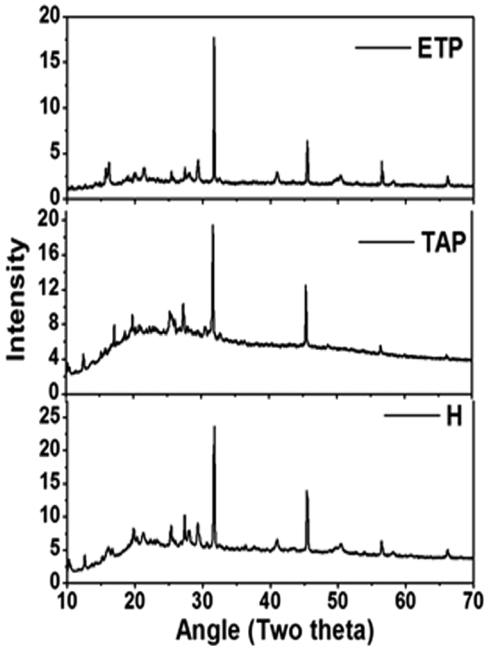

FIG. 2. XRD pattern of ETP, TAP and HC.

(υasC=C-C) and 935 cm^{-1} (C-H in plane deformation). Some other absorption peaks due to TTA are seen at 1359 cm^{-1} (υsC=O), 1279 cm^{-1} (υasCF3), 1205 cm^{-1} and 1179 cm^{-1} (βsC-H) and 642 cm^{-1} (βsCF3).[37] Characteristic peaks of phen are located at 1604 cm^{-1} (υC=N), 1509 cm^{-1} (υC=C), 1413 cm^{-1} (υC=C and υC=N), 983 cm^{-1} (δC-H), 840 cm^{-1} (δC=CH-C) and 723 cm^{-1} (δC-H).[38] Peak corresponding to the stretching vibration of Eu-O appears at 581 cm^{-1}.

On the other hand, the FTIR spectra of TAP also contains large number of vibrational peaks corresponding to its constituents namely phen, ASA and Tb-O. The peak around 1600 cm^{-1} and 1625 cm^{-1} are assigned to be stretching mode of phenyl and aspirin carboxyl group respectively. The characteristics peaks due to phen are observed at 1507 cm^{-1} (υC=C), 1396 cm^{-1} (υC=N), 842 cm^{-1} (δ δC=CH-C) and 730 cm^{-1} (δC-H).[38,39] Peak corresponding to the stretching vibration of Tb-O appears at 456 cm^{-1}. The IR peaks around 2851 and 2934 cm^{-1} are attributed to the symmetric (ν_s)

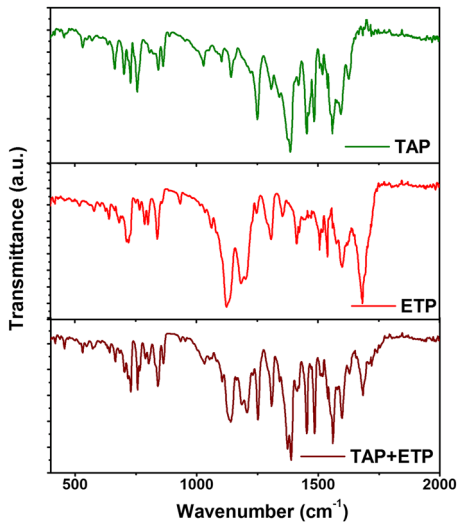

FIG. 3. FTIR spectra of TAP, ETP and HC in 400-4000 cm^{-1} region.

and asymmetric (ν_{as}) stretching vibrations of C-H. In addition the peaks around 1460 and 1570 cm^{-1} are attributed to the symmetric (ν_s) and asymetric (ν_{as}) modes of carboxylic groups (-COO-).[39] The band around 1720 cm^{-1} arises due to the stretching vibration of C=O group.

When ETP and TAP are mixed together to form HC, the peak position of hybrid does not change much, indicating the change in bond length during HC formation. These changes may arise due to weak interactions between the two complexes. There is no additional bands in HC, indicates that there is no new bond formation and the organic structure remains almost unaltered at the atomic level. Comparing the FTIR spectra of TAP, ETP with HC, the intensity of TAP band and hybrid bands (common in both) does not change much and remains almost constant. On the other hand the intensity of common ETP bands in HC reduces (1179 cm^{-1}, 1205 cm^{-1} and 1720 cm^{-1}), indicates the energy of ETP in HC reduces upto some extent, indicating the lowing in bond energy of (βsC-H) and stretching vibration of C=O group. That may stabilize the HC system. All spectra contain broad absorption bands around 3440 cm^{-1} resulting from stretching modes of OH group, but the intensity of peak reduces much more in case of HC. In case of HC, both complexes cover each other and reduce the possibility of adsorption of quenching centers from external environment.

B. Structural characterization using TEM and EDX

As AgNPs have been used to enhance the emission intensity of HC, therefore, the structural as well as optical characterization of prepared AgNPs must be carried out. Fig. 4 shows the TEM images of silver nanoparticles (scale bar: 100, 50 and 10 nm) along with the selected area electron

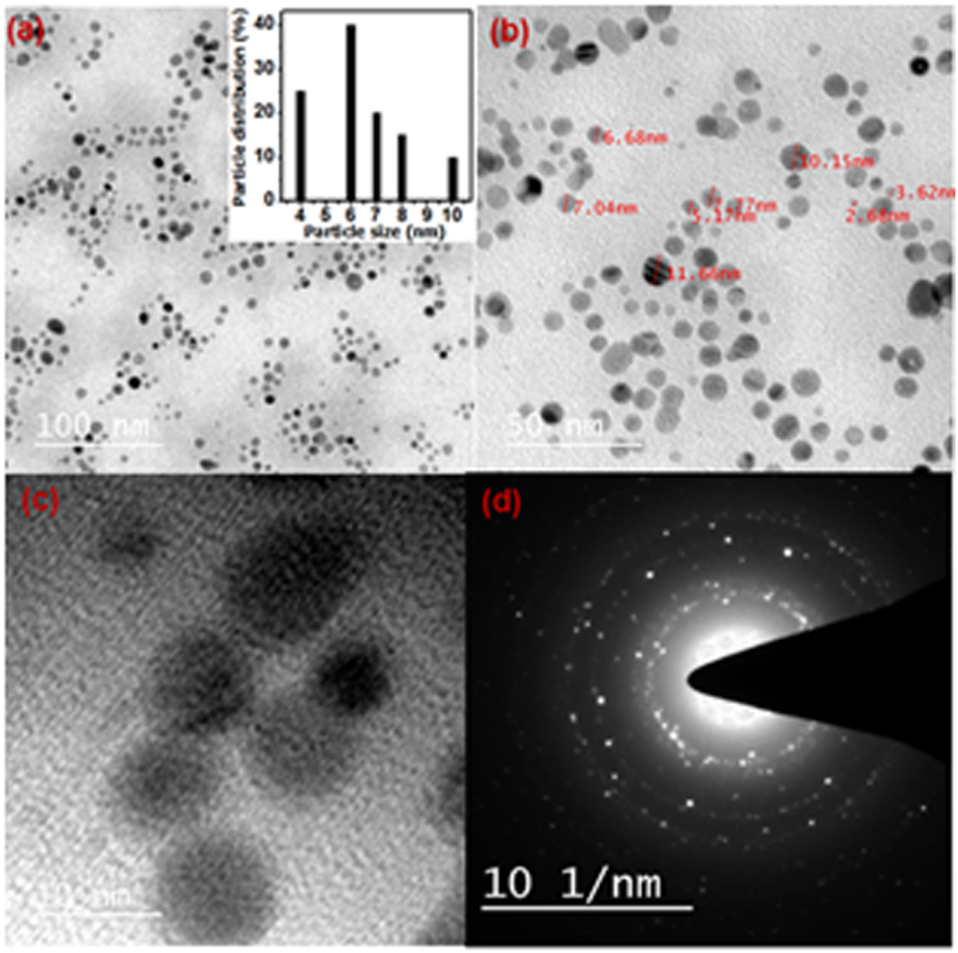

FIG. 4. **(a, b)** TEM images, the inset show the histogram of the size distribution of AgNPs. **(c)** HRTEM image and **(d)** SAED pattern of AgNPs. Inset shows the plasmonic absorption of AgNPs.

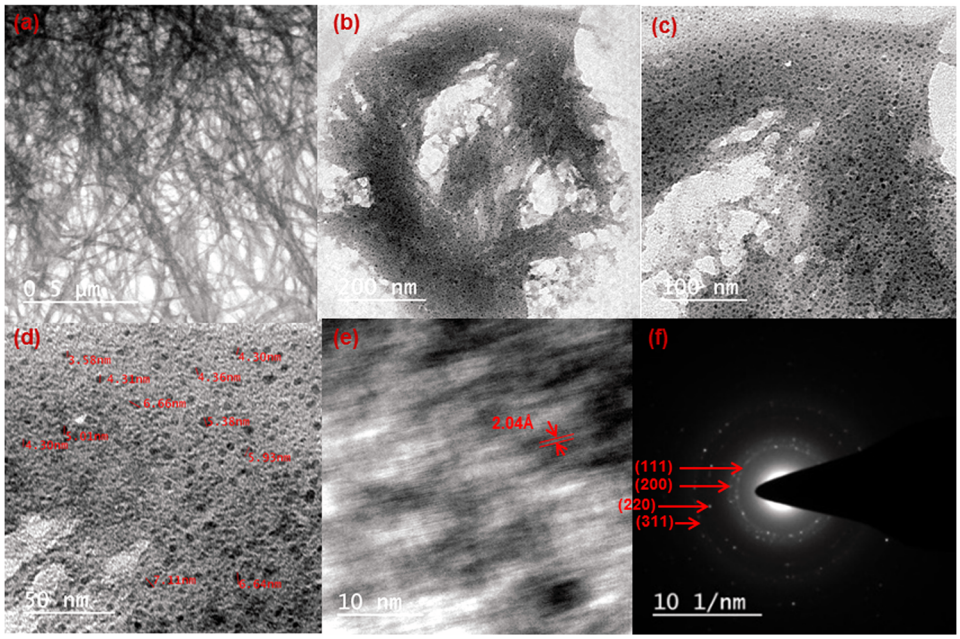

FIG. 5. **(a)** TEM image of TAP complex **(b, c, d)** TEM images **(e)** HRTEM image and **(f)** SAED pattern of AgNPs embedded HC.

diffraction (SAED) pattern. Fairly isolated nanoparticles are spherical in shape and quite uniform. The mean particle size of AgNPs was calculated using histogram plot and it was found to be 6.5 nm with the variations in particle size from 4-10 nm (inset of Fig. 4(a)). The surface plasmon resonance (SPR) absorption bands of these AgNPs have been observed around 394 nm (Inset of Fig. 4(c)). The HRTEM image (Fig. 4(c)) reveals the highly crystalline nature with an inter-planner spacing of 2.04 Å corresponding to (200) planes of face center cubic (fcc) Ag-nanostructured. The SAED patter shows the polycrystalline diffraction rings which are well matched with fcc Ag- nanocrystal structure. Thus, the TEM, HRTEM and SEAD pattern clearly demonstrates that silver nano-particles have good crystalline property along with small particle size (<10 nm).

Fig. 5(a) shows the TEM image of TAP complex, which exhibits its nano-fibrous structure. The average length and thickness of fiber are 600-1000 nm and 5-15 nm, respectively. The nanofiber structure is very dense and looks like net. Since the size of nanocrystallites is about 20 nm; that show good agreement with TEM data. Further, Fig. 5(b–c) show the TEM images of the HNPs which reveal that the silver nanoparticles are fairly dispersed on the surface of HC. The HNPs appear with high density and tree like structure as ETP is bulky in nature and covers nano-fibrous TAP complex completely as if TAP has been coated with the layer of ETP. The bulky nature of HNPs in presence of ETP opens the possibility of physical interactions (weak interactions between the two complexes like van der Walls interaction). The HRTEM image of HNPs shows the presence of lattice fringes corresponding to AgNPs, see in Fig. 5(e). In Fig. 5(f), the SAED pattern of HNPs shows set of diffraction rings from AgNPs. Figure S1 of the supplementary material shows the EDAX spectrum of the HC for detailed elemental analysis. The EDX pattern shows the peaks corresponding to europium, terbium, sodium, fluorine, oxygen, carbon, sulfur, chlorine giving the evidence for the presence of ETP as well as TAP in HC. Again Fig. S2 of the supplementary material demonstrated the attachment of AgNPs with HC in HNPs. EDX pattern of HNPs yielded peaks corresponding to the Ag elemental.

V. OPTICAL CHARACTERIZATIONS

A. Photoluminescence/excitation (PL/E)

The PLE spectrum of TAP complex monitored at 544 nm emission wavelength shows broadband excitation consisting of two maxima ranging in between 240-380 nm in UV region (as shown in

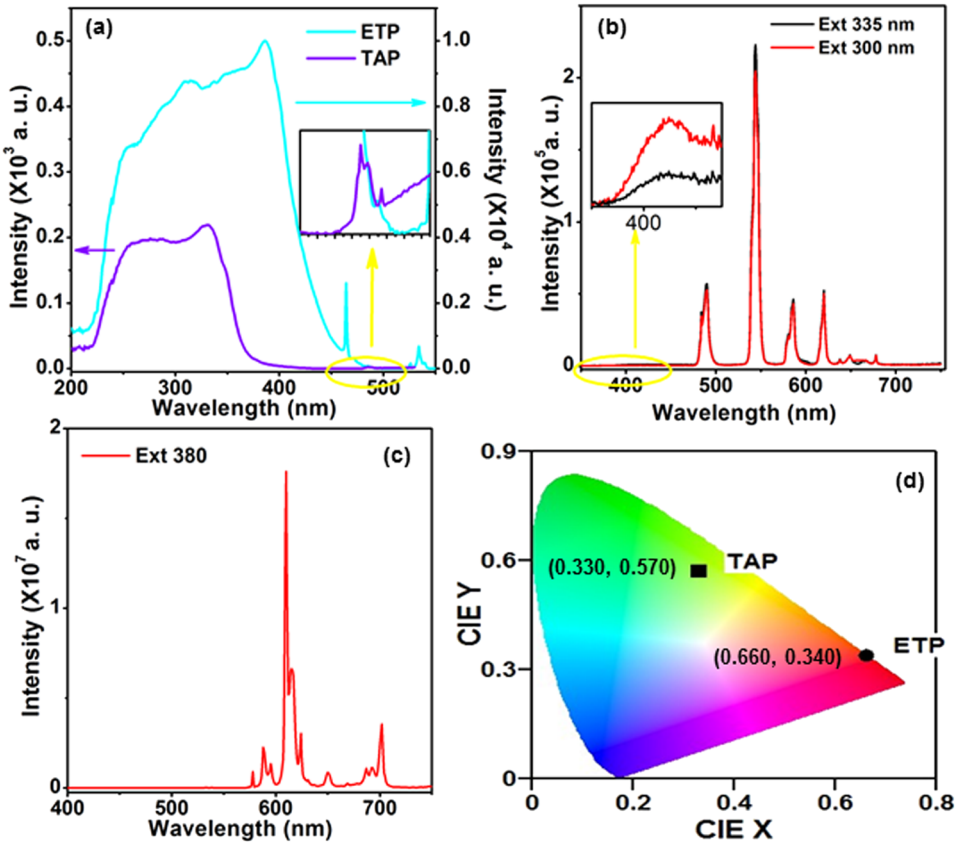

FIG. 6. **(a)-** PLE spectra of ETP (λ_{em}=611 nm) and TAP (λ_{em}=544 nm) complex, **(b)-** PL spectra of TAP for λ_{ex}=300 nm and 335 nm, **(c)**- PL spectra of ETP under 380 nm excitation, and **(d)-** CIE plot of the ETP and TAP complex showing orange and green emission respectively.

Fig. 6(a)). The spectrum reveals the presence of two excited states of TAP complex with their peak maxima at 275 nm and 335 nm respectively. One of them is due to π-π* transition and other is due to n-π transition of TAP. The maximum absorption at 335 nm is due to the overlapping of ASA absorption band with Tb^{3+} absorption peak ($^7F_6 \rightarrow {}^5D_1$) while the other maxima at 275 nm arises by overlapping of ASA and Phen absorptions. Besides this broadband, one additional sharp peak at 485 nm is also present and this is the characteristics excitation band of Tb^{3+} ion due to $^7F_6 \rightarrow {}^5D_4$ transition. Fig. 6(b) shows the PL spectrum of emission bands due to ASA and Tb^{3+} both. Upon excitation with 300 and 335 nm wavelengths, the broad emission band of ASA appears in the range of 390-450 nm along with the bands of Tb^{3+}. The intensity of ASA emission upon 300 nm excitation is higher than that of the emission intensity at 335 nm excitation. In contrast, PL emission intensity of Tb^{3+} ion is 1.3 times larger at 335 nm excitation than that of 300 nm. The lower emission intensity of ASA, upon 335 nm wavelength excitation, indicates the relatively higher migration of energy from band-edge of ASA to Tb^{3+} ion (shown in inset of Fig. 6(b)). The energy transfer process is further studied using time domain measurements. Other emission bands of Tb^{3+} ions have been observed at 488, 544, 586, 620, 649, 667 and 678 nm wavelengths due to the $^5D_4 \rightarrow {}^7F_6$, $^5D_4 \rightarrow {}^7F_5$, $^5D_4 \rightarrow {}^7F_4$, $^5D_4 \rightarrow {}^7F_3$, $^5D_4 \rightarrow {}^7F_2$, $^5D_4 \rightarrow {}^7F_1$ and $^5D_4 \rightarrow {}^7F_0$ transitions, respectively.[27,40–42] Amongst all these emissions, the induced electric dipole transition $^5D_4 \rightarrow {}^7F_5$ at 544 nm appears with highest intensity.

The emission spectra recorded on excitation with different wavelengths (260, 300, 335, 380 and 488 nm) shows maximum emission intensity of Tb^{3+} ion upon 335 nm excitation (shown in Figure S3 of the supplementary material). The emission spectrum of $TbCl_3.6H_2O$ on 335 nm excitation exhibits all characteristic emission bands of Tb^{3+} with low intensity, in fact the emission intensity reduces up to 50 times as compared with TAP as shown in Figure S4 of the supplementary material. This observation again indicates feeding of energy to Tb^{3+} ion via organic components of TAP.

The excitation spectrum of ETP monitored at λ_{em}= 611 nm shows even broader excitation band in the range of 240-480 nm (shown in Fig. 6(a)). Along with this broad excitation, some sharp characteristic excitation peaks of Eu^{3+} due to $^7F_0 \rightarrow {}^5D_2$ and $^7F_0 \rightarrow {}^5D_1$ transitions at 464 and 532 nm wavelengths are also present (see Fig. 6(a)). The emission intensity of ETP is maximum at 380 nm. The detailed study of ETP is given in our previous reports.[6,28]

The PL spectrum of ETP (shown in Fig. 6(c)) consists of emission bands of Eu^{3+} at 578, 589, 611, 650 and 700 nm due to the transitions from the excited energy state $^5D_0$ to the different ground states ^7F_j viz. $^5D_0 \rightarrow {}^7F_0$, $^5D_0 \rightarrow {}^7F_1$, $^5D_0 \rightarrow {}^7F_2$, $^5D_0 \rightarrow {}^7F_3$, and $^5D_0 \rightarrow {}^7F_4$, respectively.[43–45] The hypersensitive transition at 611 nm possesses the highest intensity and the intensity of rest of emission bands is relatively very low. This is due to the asymmetry created by organic ligands (TTA and Phen) around the Eu^{3+} ion. Unlike TAP, upon excitation with 380 nm, ETP does not show any emission of TTA (organic ligand), rather it transfers its total energy to Eu^{3+} ions which gives intense orange-red emission.[6] Fig. 6(d) exhibits the color co-ordinates of TAP and ETP complexes which are (0.33, 0.57) and (0.66, 0.34), respectively. The absolute quantum yield of the ETP is very high with numerical value as 88.9%. This suggests that ligands are transferring almost entire of its energy to the central Eu^{3+} ions.

The excitation spectra of HC (see Fig. 7(a)) were recorded by monitoring emission at 544 nm and 611 nm (corresponding to maximum emission intensities of Tb^{3+} and Eu^{3+} ions). The PLE corresponding to 544 nm emission of Tb^{3+} ions, carries a broad band absorption (240-390 nm) due to ASA and sharp absorption of Tb^{3+} at 486 nm like TAP excitation spectrum. The broadening in excitation spectra of the HC are occurring due to the combine spectra of ETP and TAP. On the

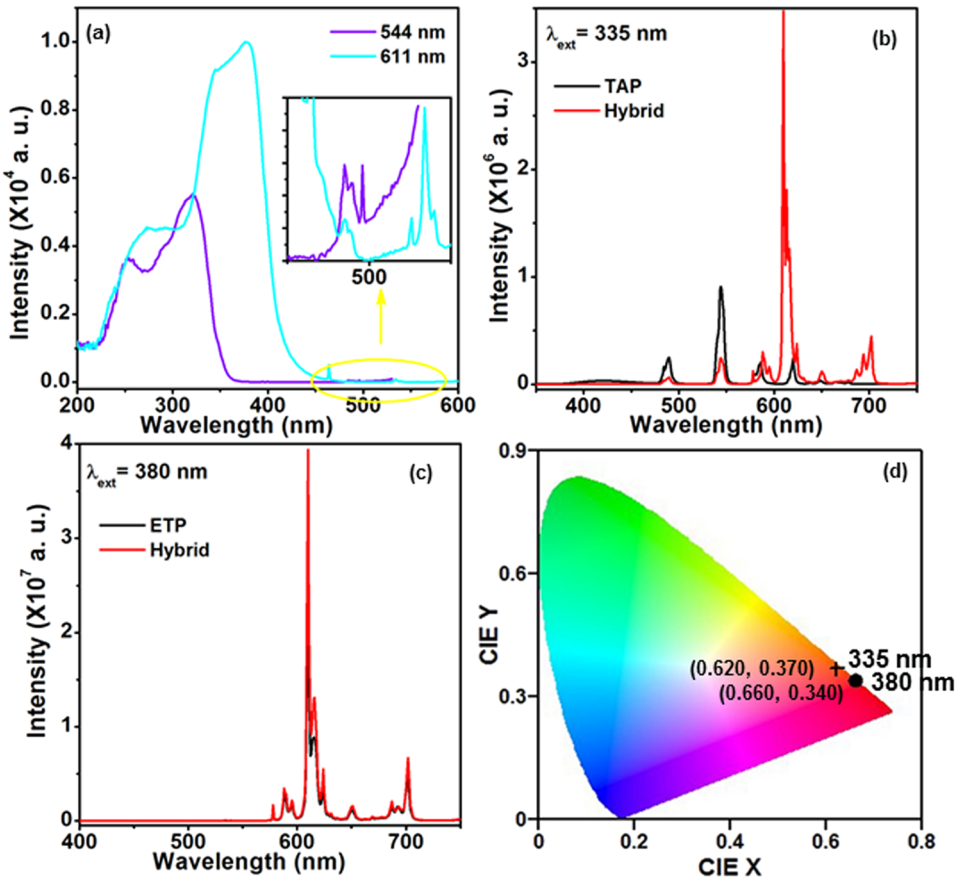

FIG. 7. **(a)-** PLE spectra of HC for λ_{em}=611 and 544 nm, **(b)-** PL spectra of TAP and HC under 335 nm excitation, **(c)**- PL spectra of ETP and HC under 380 nm excitation, and **(d)-** CIE plot of the HC showing orange red emission under 335 and 380 nm under excitations respectively.

other hand, the PLE corresponding to 611 nm emission of Eu^{3+} ions carries broad band absorption (240-490 nm) of TTA as well as Phen and sharp absorption bands due to Eu^{3+} at 464 nm, 532 nm and 582 nm. Besides these bands, interestingly, two more sharp absorption bands are also seen at 486 and 586 nm wavelengths, which are not characteristics of Eu^{3+} ion. These bands are necessarily the characteristics absorption bands of Tb^{3+} ion as observed in TAP absorption. To monitor emission spectra, we have chosen 335 and 380 nm excitation wavelengths. The emission spectrum of HC contains emission spectrum of both Tb^{3+} and Eu^{3+} ion on excitation with 335 nm and 380 nm wavelengths as shown in Fig. 7(b and c) respectively. The emission wavelengths are 486, 544, 588, 620 and 678 nm for the transitions from $^5D_4 \rightarrow {}^7F_6$, $^5D_4 \rightarrow {}^7F_5$, $^5D_4 \rightarrow {}^7F_4$, $^5D_4 \rightarrow {}^7F_3$, $^5D_4 \rightarrow {}^7F_2$ and $^5D_4 \rightarrow {}^7F_1$ respectively, for Tb^{3+} ion and 532, 586, 591, 611, 650 and 700 nm for the transitions from $^5D_1 \rightarrow {}^7F_1$, $^5D_0 \rightarrow {}^7F_0$, $^5D_0 \rightarrow {}^7F_1$, $^5D_0 \rightarrow {}^7F_2$, $^5D_0 \rightarrow {}^7F_3$, and $^5D_0 \rightarrow {}^7F_4$ respectively of Eu^{3+} ions. The presence of emission bands of both the complexes signifies the characteristics emission of HC. The emission spectra of HC is quite different from both the TAP and ETP complexes, in fact it shows an energy transfer from Tb^{3+} to Eu^{3+} as well as ASA to TTA viz. the energy transfer from TAP to ETP complex, where energy transfer takes place from Tb^{3+} to Eu^{3+} ion through indirect process. The singlet state emission of ASA (as it is present in isolated TAP emission) is totally missing in HC and thus, this indicates the transfer of energy from ASA to TTA through non-radiative process as emission of ASA overlaps with excitation spectrum of ETP (Fig. 7(b)) On exciting HC with 335 nm wavelength as shown in Fig. 7(b), the emission bands of Tb^{3+} in TAP complex suppresses by almost 65% in HC with respect to the integrated emission intensity of same in TAP, at the same time the integrated intensity of emission bands of Eu^{3+} ions in HC enhances by almost 40% as compared with the fluorescence intensity of Eu^{3+} ion in ETP as shown in Fig. 6(c). The one more important observation in the case of HC is disappearance of emission bands due to the ASA and decrease in the overall emission of Tb^{3+} ion in TAP complex. The disappearance of ASA does not indicate any direct energy transfer to Eu^{3+}, as there is an overlap of emission spectrum of ASA with the absorption spectrum of ETP and this may be responsible for non-radiative energy transfer from ASA to Eu^{3+} due to induced electric dipole-quadrupole interaction. The other way of energy transfer is from singlet state of ASA to the singlet state of TTA (due to spectral overlapping of absorption spectra) and in next step the energy of TTA is transferred to Eu^{3+} ion through triplet state and hence it indicates the indirect energy transfer from ASA to Eu^{3+} ion and these are the possible ways of energy transfer. The other excitation wavelength is 380 nm, where the emission of Tb^{3+} ion almost disappears and only the emission due to Eu^{3+} ion is present. The reason behind this is the absence of absorption of TAP complex as well as Tb^{3+} ion at this wavelength. At 380 nm excitation wavelength, the absorption of ETP is the maximum and hence only the Eu^{3+} ion emission dominates on this particular excitation wavelength. The overall emission spectra of HC indicate the migration of energy from TAP to ETP either directly or through indirect process.

The CIE coordinates of HC on excitation with both wavelengths (335 and 380 nm) appear in red region with color coordinates as (0.62, 0.37) and (0.66, 0.34) respectively. The change in color coordinates from (0.33, 0.57) to (0.62, 0.37) in TAP and HC at 335 nm excitation wavelength, also verify the energy transfer from Tb^{3+} to Eu^{3+}. Upon excitation with 380 nm wavelength, the color coordinates do not change, indicating no energy transfer. The integrated quantum yield of the HC is higher than that of the integrated quantum yield of ETP and is found to be 90.6±10 %.

B. Energy transfer mechanism and decay dynamics

The energy transfer mechanism has been shown in energy level diagram (see Fig. 8). In case of ETP complex, TTA and Phen absorb UV energy strongly and transfers it to Eu^{3+} ions through triplet state of TTA to the $^5D_2$ level of Eu^{3+} ion and through singlet state S_1 to $^5D_3$ energy state of Eu^{3+}.[6] While S_1 and T_1 of ASA transfers its energy to Tb^{3+} ion in case of TAP complex.[27]

The energy transfer mechanism in HC are different from both in which singlet state (S_1) of TAP transfers its energy to singlet state (S_1) of TTA and $^5D_4$ state of Tb^{3+} also transfers its energy to $^5D_1$ energy state of Eu^{3+}. This mechanism shows the transfer of energy from Tb^{3+} to Eu^{3+}. This can be further verified by the decay dynamics. The decay dynamics of TAP complex has been carried out by monitoring the Tb^{3+} ion emission wavelength at 544 nm upon 335 and 380 nm excitations. The decay profile measurement upon both excitation wavelengths (335 and 380 nm) shows single exponential

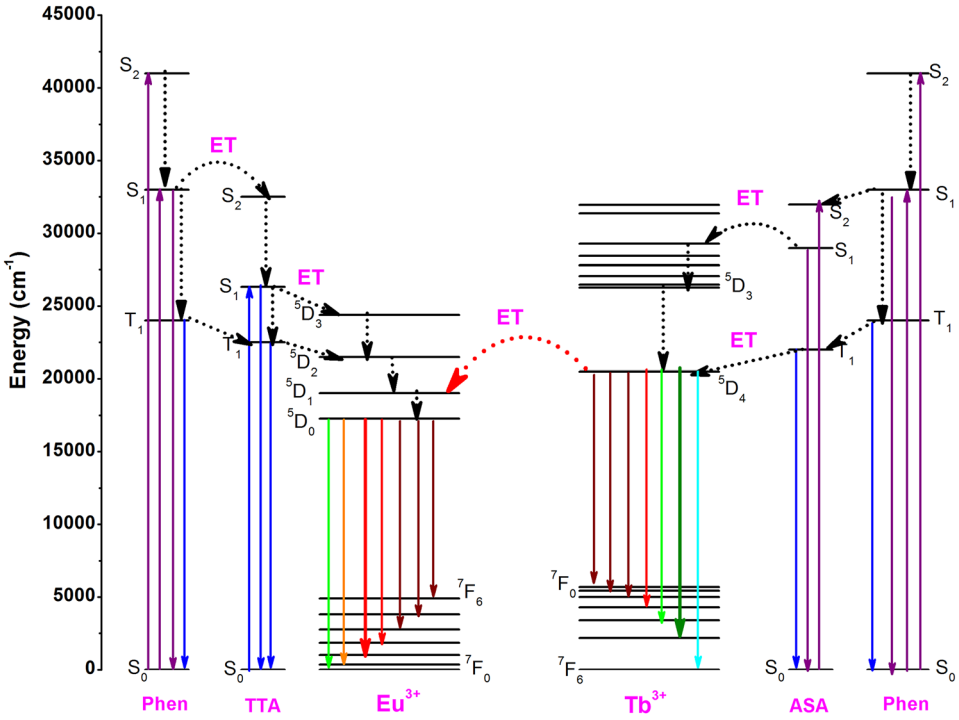

FIG. 8. The energy level diagram showing the mechanism of energy transfer in ETP, TAP and HC.

fitting with consecutive life times of 1154±6 μs and 815±4 μs and the $\chi^2_=$ for both cases are more than 0.99. The reason in the difference of life times is the overlapping of absorption spectrum of ASA and Tb^{3+} ion for 335 nm excitation. The strong coupling between ASA and Tb^{3+} provides higher possibility of energy transfer upon 335 nm excitation rather than 380 nm excitation (see Fig. 9(a) and (c)). Further the lifetime of Eu^{3+} ion in ETP remains unaltered with 1342±9 μs upon excitation with 335 nm and 380 nm excitation wavelengths (see Fig. 9(b) and (d)), again with exponential fitting values more than 0.99.

The hybrid material of ETP and TAP complexes gives some interesting results. The decay profile study contains two excitation wavelengths (335 and 380 nm) as well as two emission wavelengths (544 and 611 nm), hence four decay profiles have been taken under consideration. The prime reason for choosing these two excitation wavelengths is to search the possibility of energy migration in presence of two isolated rare-earth entities, as these two wavelengths are correspondingly overlapped wavelengths of rare-earths which overlap with their respective complex excitation wavelengths. Upon exciting the HC with 335 nm wavelengths, the life time of Tb^{3+} and Eu^{3+} ions as monitored at 544 and 611 nm wavelengths results 835±6 μs and 1532±11 μs respectively. At the same time, lifetime is found to be 657±8 μs and 1379±9 μs respectively for 380 nm excitation wavelength. Therefore the lifetime of Tb^{3+} in HC is decreased from 1154 μs to 835 μs by 27.6% (319 μs) with respect to the lifetime of Tb^{3+} in TAP for 335 nm excitation and 544 nm emission wavelengths. The migrated energy efficiency can be calculated by the relation[46,47] -

$$\eta = 1 - \frac{\tau 1}{\tau 2} \tag{1}$$

Where η is the fraction if energy migrated and τ_1 and τ_2 are the lifetime Tb^{3+} ion of HC and TAP complex. For 335 nm excitation and 544 nm emission wavelengths, the fraction of energy migration in case of HC is 0.276 or 27.6%.

While at the same time the life time of Eu^{3+} in ETP and HC are found to be 1342 μs and 1532 μs respectively for 335 nm excitation and 611 nm emission wavelengths. This suggests that Eu^{3+} ions in HC gain energy. This gain is again calculated with the above mentioned equation and found to be 14.2%. Therefore Tb^{3+} ion releases 27.6% of its photon in case of HC, while only 14.2% is

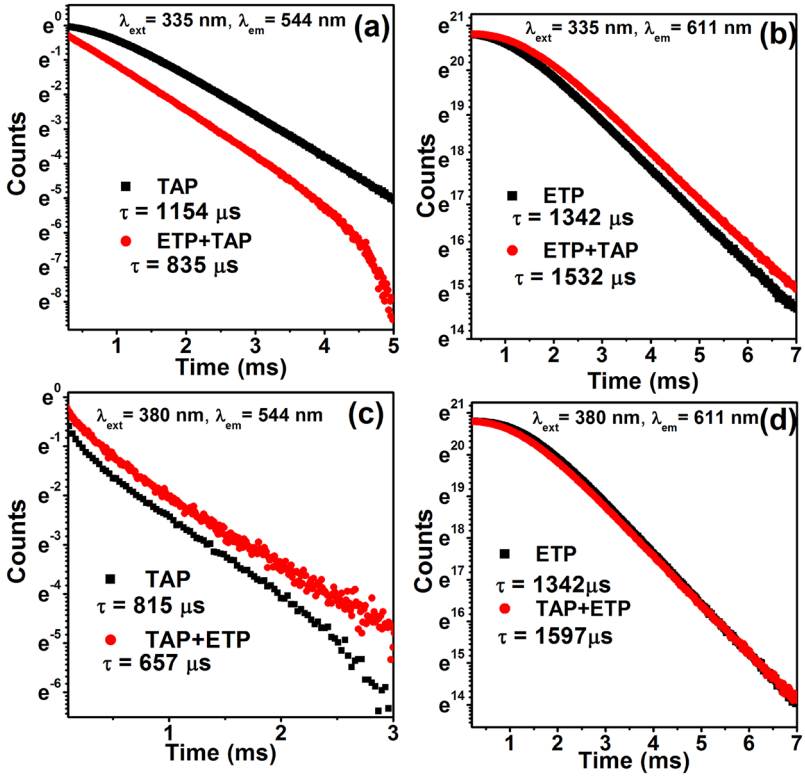

FIG. 9. **(a, c)** Decay profile $^5D_4 \rightarrow {}^7F_5$ transition of Tb^{3+} in TAP and HC under 335 and 380 nm excitation respectively, **(b-d)** Decay profile of $^5D_0 \rightarrow {}^7F_2$ transition of Eu^{3+} in ETP and HC under 335 and 380 nm excitation, respectively.

gained by Eu^{3+} ion of HC. Therefore the rest of photo energy is thus lost in non-radiative process as the structure is very bulky and the high phonon energy (as suggested by FTIR spectra) reduces the efficiency of energy transfer.

VI. EFFECT OF SILVER (Ag) NANOPARTICLES

Fig. 10 represents the effect of AgNPs addition on the excitation and emission spectra of HC. The excitation spectra of AgNPs embedded HC (λ_{em}= 611 nm) shows enhancement in the excitation band (240-480 nm) with respect to complex without AgNPs. This enhancement is due to the plasmonic band of Ag nanoparticles, which overlaps with Eu-Tb complex absorption (absorption spectra of AgNPs is shown in Fig. S5 of the supplementary material). Therefore the excitation spectra of HNPs are basically the combination of AgNPs and the HC. The PLE and PL spectra up to 1 ml AgNPs concentration shows an increment of 28% in their relative emission intensity with respect to the complex without AgNPs. The possible mechanism for improvement in the PLE and PL signal in presence of AgNPs, is associated with the increase in the intensity of the local electric field near the edge of nanoparticles, which significantly influence the fluorescence behavior of neighboring emitting centers. The AgNPs concentrate the incident light to improve the excitation intensity of the complex. At the same time, it can also facilitate the energy transfer from ligands to lanthanide ions. Another factor which may influence the emission intensity is that, the AgNPs can increase the radiative decay rates of lanthanides to improve the fluorescence intensity. To verify the plasmonic effect, the lifetime measurements of HC with and without AgNPs have been carried out. The fluorescence decay time and quantum yield of the emitter are given as-

$$\tau = 1/(\Gamma + k_{nr}) \text{ and } Q = \Gamma/(\Gamma + k_{nr}) \text{ respectively.}$$

where Γ and k_{nr} are radiative and non-radiative decay rates, respectively. Let Γ_m be the radiative decay rate due the presence of metal nanoparticles. Therefore, new fluorescence decay time and

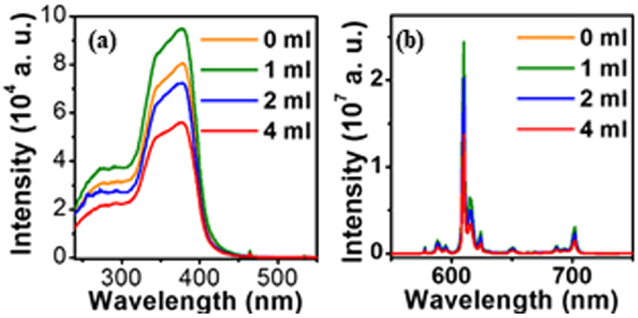

FIG. 10. **(a, b)** PLE (λ_{em}=611 nm) and PL (λ_{ext}= 380 nm) spectra of HC with different concentrations of AgNPs.

quantum yield is given by-

$$\tau = 1/(\Gamma + k_{nr} + \Gamma_m) \text{ and } Q = (\Gamma + \Gamma_m)/(\Gamma + k_{nr} + \Gamma_m) \text{ respectively}$$

Hence the above equations predict that, the increase in radiative decay rates increases the quantum yields while the life time decreases. Fig. S6 of the supplementary material shows that, addition of AgNPs does not cause any significant reduction in the lifetime. But still in all cases, lifetime slightly decreases. Hence an increase in fluorescence intensity with a very small change in decay time can be explained by modification in excitation rates. For higher concentration of AgNPs (2 and 4 ml), intensity of excitation as well as emission peaks reduces due to reabsorption of surface plasmon.

VII. TEMPERATURE SENSING

The sensitive temperature PL dependence of the samples studied here opens the opportunity to use this material as temperature sensor. Temperature sensing in ETP is already demonstrated by Shahi et al. and found that sensitivity in ETP is very high as compared to others.[48–51] The ligand ASA in TAP has already been used for medical applications as ASA is not toxic. TAP along with ETP could be a new material for biomedical and imaging purposes, particularly for cancer treatment as temperature nearby the cancer cell shows higher temperature than other part of human body. To see the effect of temperature for TAP with ETP in HNPs, The most intense hypersensitive transition at 611 nm of Eu^{3+} ($^5D_0 \rightarrow {}^7F_2$) has been considered to monitor the effect of temperature. For the demonstration of temperature sensing behavior of HNPs, the PL intensity at 611 nm, i.e., the $^5D_0 \rightarrow {}^7F_2$ transition of the

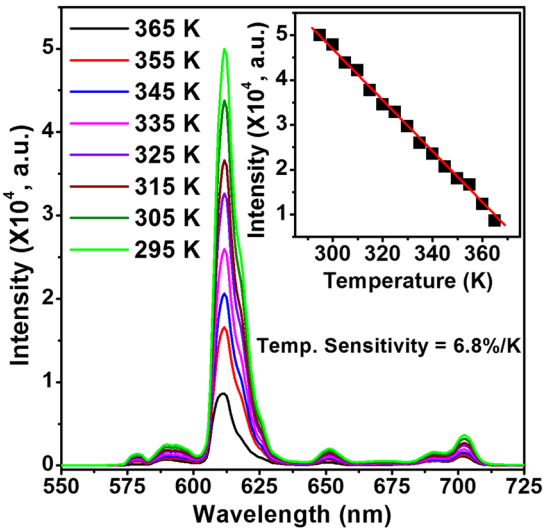

FIG. 11. Temperature sensing of HNPs in between 295-365 K. Sensitivity was found to be 6.8 %/K.

Eu^{3+} ion, versus temperature have been monitored. Fig. 11 shows PL spectra of HNPs at various temperatures in the range of 365 to 295 K. It shows, as the temperature of the sample decreases, the PL intensity notably increases and it shows almost linear dependence on temperature in this region. A temperature decrease from 365 to 295 K induces the PL intensity increases by a factor of ~4.8 because, most likely, of the decrease in non-radiative relaxation channels by damping some of the vibronic modes during the cool down. Important for the envisaged application is the fact that the signal changes are fully reversible. The temperature sensitivity can be expressed as % change in PL intensity per K, i.e. by the expression $\Delta I/(I_{ref}.\Delta T)$), where I_{ref} is the PL intensity at 305 K, ΔT is the change in temperature, and ΔI is the PL intensity variation corresponding to ΔT. The average temperature sensitivity is found to be 6.8% per K, which is significantly very high to our previous report and could be processed for biological imaging.[6] In our work since PL vs temperature curve shows an excellent linear fit (χ^2=0.99), the temperature sensitivity is nearly constant in the measured temperature range 365-295K, therefore it has better prospect for application point of view. The advantages of this temperature sensor are being noninvasive, accurate, and capable to operate even in strong electromagnetic field.

VIII. CONCLUSION

Here two β-diketonate complexes have been mixed in cyclohexane by heavy ultra-sonication. The hybrid material thus obtained, exhibit the energy transfer from ligand to ligand and ligand to central metal ion and central metal ion (Tb^{3+}) to central metal ion (Eu^{3+}). The PLE and PL emission shows excellent optical properties and energy transfer from Tb^{3+} to Eu^{3+}. The energy transfer can further be verified by lifetime measurement, which shows decrement in lifetime of Tb^{3+} in HC with respect of TAP, whereas the increase in life time of Eu^{3+} in HC with respect to ETP. The addition of Ag nanoparticles further enhances the fluorescence of Eu^{3+} in HC. This hybrid material is further used for luminescent thermometry and the sensitivity is found to be 6.8% change in signal, which is quite high. This material can be used for bio-medical and imaging application as ASA is already used as medicine and TAP is also nontoxic.

SUPPLEMENTARY MATERIAL

See supplementary material for Fig. S1 and S2 show EDX patterns of HC and HC@AgNPs for elemental analysis, showing the attachment of Eu/Tb/AgNPs respectively. Fig. S3 show emission spectra of TAP and different excitation wavelength. Fig. S4 show comparative emission spectra of TAP and $TbCl_3.6H_2O$ on 335 nm excitation wavelength. Plasmonic absorption band is shown in Fig. S5. Fig. S6 show decay profile at different excitation wavelength on AgNPs addition.

ACKNOWLEDGMENTS

This work is also supported by the DST project 445 (project no. SR/S2/LOP/0023/2012) to S.B.R. in India.

[1] L. D. Carlos, R. A. S. Ferreira, V. d. Z. Bermudez, B. J. López, and P. Escribano, Chem. Soc. Rev. **40**, 536–549 (2011).
[2] P. P. Sun, J. P. Duan, H. T. Shih, and C. H. Cheng, Appl. Phys. Lett. **81**, 792–794 (2002).
[3] J. Rocha, L. D. Carlos, F. A. A. Paza, and D. Ananias, Chem. Soc. Rev. **40**, 926–940 (2011).
[4] P. Escribano, B. J. López, J. P. Arago, E. Cordoncillo, B. Viana, and C. Sanchez, J. Mater. Chem. **18**, 23–40 (2008).
[5] M. Shibasaki and N. Yoshikawa, Chem. Rev. **102**, 2187–2209 (2002).
[6] P. K. Shahi, A. K. Singh, S. K. Singh, S. B. Rai, and B. Ullrich, ACS Appl. Mater. Interfaces **7**, 18231–18239 (2015).
[7] C. D. Brites, P. P. SLima, N. J. O. Silva, A. Millán, V. S. Amaral, F. Palacio, and L. D. Carlos, Adv. Mater. **22**, 4499–4504 (2010).
[8] A. Picot, A. D. Aleo, P. L. Baldeck, A. Grichine, A. Duperray, C. Andraud, and O. Maury, J. Am. Chem. Soc. **130**, 1532–1533 (2008).
[9] L. D. Carlos, R. A. S. Ferreira, V. d. Z. Bermudez, and S. J. L. Ribeiro, Adv. Mater. **21**, 509–534 (2009).
[10] W. Liu, T. Jiao, Y. Li, Q. Liu, M. Tan, H. Wang, and L. Wan, J. Am. Chem. Soc. **126**, 2280–2281 (2004).
[11] N. Liu, W. Qin, G. Qin, T. Jiang, and D. Zhao, Chem. Commun. **47**, 7671–7673 (2011).
[12] Y. L. Wang, N. M. Estakhri, A. Johnson, H. Y. Li, L. X. Xu, Z. Zhang, A. Alù, Q. Q. Wang, and C. K. Shih, Sci. Rep. **5**, 10196 (2015).
[13] Y. Wang, F. Nan, Z. Cheng, J. Han, Z. Hao, H. Xu, and Q. Wang, Nano Res. **8**(9), 2970–2977 (2015).

[14] W. Xu, Y. Zhu, X. Chen, J. Wang, L. Tao, S. Xu, T. Liu, and H. Song, Nano Res. **6**(11), 795–807 (2013).
[15] S. Parola, B. J. López, L. D. Carlos, and C. Sanchez, Adv. Funct. Mater. **26**, 6506–6544 (2016).
[16] K. Binnemans, Chem. Rev. **109**, 4283–4374 (2009).
[17] A. M. Kłonkowski, S. Lis, M. Pietraszkiewicz, Z. Hnatejko, K. Czarnobaj, and M. Elbanowski, Chem. Mater. **15**, 656–663 (2003).
[18] W. Yan, L. Wang, K. Yangxiao, Z. Fu, and T. Wu, Dalton Trans. **45**, 4518–4521 (2016).
[19] J. Yang, L. Zhou, L. Yuan, X. Zhou, B. Hu, X. Zhang, and S. Hua, New J. Chem. **40**, 7350–7358 (2016).
[20] W. Chen and S. Fukuzumi, Inorg. Chem. **48**, 3800–3807 (2009).
[21] J. Wang, R. Wang, J. Yang, Z. Zheng, M. D. Carducci, T. Cayou, N. Peyghambarian, and G. E. Jabbour, J. Am. Chem. Soc. **123**, 6179–6180 (2001).
[22] T. Zhang, Z. Xu, L. Qian, F. Teng, X. R. Xu, and D. L. Tao, J. Appl. Phys. **98**, 063503-1–063503-4 (2005).
[23] L. Yuguang, Z. Jingchang, C. Weiliang, Z. Fujun, and X. Zheng, J. Rare Earths **25**, 296–301 (2007).
[24] P. K. Shahi, P. Singh, A. K. Singh, S. K. Singh, S. B. Rai, and R. Prakash, J. Colloid Interface Sci. **491**, 199–206 (2017).
[25] P. K. Shahi, P. Singh, and S. B. Rai, J. Phys. D: Appl. Phys. **50**, 075501 (2017).
[26] Z. Chen, B. Zhao, P. Cheng, X. Q. Zhao, W. Shi, and Y. Song, Inorg. Chem. **48**(8), 3493–3495 (2009).
[27] B. Kumar, G. Kaur, and S. B. Rai, Journal of Photochemistry and Photobiology A: Chemistry **332**, 413–421 (2017).
[28] P. Singh, P. K. Shahi, S. K. Singh, A. K. Singh, M. K. Singh, R. Prakash, and S. B. Rai, Nanoscale **9**, 696–705 (2017).
[29] F. Xie, J. S. Pang, A. Centeno, M. P. Ryan, D. J. Riley, and N. M. Alford, Nano Res. **6**(7), 496–510 (2013).
[30] S. Eustis and M. A. E. Sayed, Chem. Soc. Rev. **35**, 209–217 (2006).
[31] D. Yin, L. Zhang, X. Cao, Z. Chen, J. Tang, Y. Liu, T. Zhang, and M. Wu, Dalton Trans. **45**, 1467–1475 (2016).
[32] Q. Wang, F. Song, S. Lin, J. Liu, H. Zhao, C. Zhang, C. Ming, and E. Y. Pun, Opt Express **19**(8), 6999–7006 (2011).
[33] H. Li, J. Kang, J. Yang, and B. Wu, J. Phys. Chem. C **120**, 16907–16912 (2016).
[34] L. Sudheendra, V. Ortalan, S. Dey, N. D. Browning, and I. M. Kennedy, Chem. Mater. **23**, 2987–2993 (2011).
[35] X. Fang, H. Song, L. Xie, Q. Liu, H. Zhang, X. Bai, B. Dong, Y. Wang, and W. Han, J. Chem. Phys. **131**, 054506-1–054506-7 (2009).
[36] S. D. Solomon, M. Bahadory, A. V. Jeyarajasingam, S. A. Rutkowsky, and C. Boritz, J. Chem. Educ. **84**(2), 322–325 (2007).
[37] B. A. Uzoukwu, Inorg. Chim. Acta **I76**, 143–148 (1990).
[38] M. E. Amane and H. E. Hamdani, Int. J. Chem. Tech. Res. **6**, 465–473 (2014).
[39] M. Champeau, J. M. Thomassin, C. Jeromeb, and T. Tassaing, Analyst **140**, 869–879 (2015).
[40] P. Singh, P. K. Shahi, S. K. Singh, and S. B. Rai, J. Alloys Compd. **681**, 477–485 (2016).
[41] W. W. Holloway, Jr., M. Kestigian, and R. Newman, Phys. Rev. Lett. **11**, 458–460 (1963).
[42] A. Beeby, S. Faulkner, D. Parker, and J. A. G. J. Williams, Chem. Soc., Perkin Trans. **2**, 1268–1273 (2001).
[43] P. K. Shahi, A. K. Singh, S. B. Rai, and B. Ullrich, Sens. Actuators, A **222**, 255–261 (2015).
[44] T. Kuo, W. Lai, C. Li, Y. Wun, H. Chang, J. Chen, P. Yang, and C. Chen, Nano Res. **7**(5), 658–669 (2014).
[45] M. Yu, J. Su, G. Wang, and Y. Li, Nano Res. **9**(8), 2338–2346 (2016).
[46] P. K. Shahi, P. Singh, S. B. Rai, and A. Bahadur, Inorg. Chem. **55**, 1535–1541 (2016).
[47] M. Xiao and P. R. Selvin, J. Am. Chem. Soc. **123**, 7067–7073 (2001).
[48] P. Singh, P. K. Shahi, A. Rai, A. Bahadur, and S. B. Rai, Optical Materials **58**, 432–438 (2016).
[49] A. K. Singh, P. K. Shahi, S. B. Rai, and B. Ullrich, RSC Adv. **5**, 16067–16073 (2015).
[50] H. Peng, M. I. J. Stich, J. Yu, L. Sun, L. H. Fischer, and O. S. Wolfbeis, Adv. Mater. **22**, 716–719 (2010).
[51] S. N. Zhao, L. J. Li, X. Z. Song, M. Zhu, Z. M. Hao, X. Meng, L. L. Wu, J. Feng, S. Y. Song, C. Wang, and H. J. Zhang, Adv. Funct. Mater. **25**, 1463–1469 (2015).